

Consistent geographical patterns of changes in high-impact European heatwaves

E. M. Fischer^{1,2*} and C. Schär¹

Climate-change projections suggest that European summer heatwaves will become more frequent and severe during this century^{1–4}, consistent with the observed trend of the past decades^{5,6}. The most severe impacts arise from multi-day heatwaves, associated with warm night-time temperatures and high relative humidity. Here we analyse a set of high-resolution regional climate simulations and show that there is a geographically consistent pattern among climate models: we project the most pronounced changes to occur in southernmost Europe for heatwave frequency and duration, further north for heatwave amplitude and in low-altitude southern European regions for health-related indicators. For the Iberian peninsula and the Mediterranean region, the frequency of heatwave days is projected to increase from an average of about two days per summer for the period 1961–1990 to around 13 days for 2021–2050 and 40 days for 2071–2100. In terms of health impacts, our projections are most severe for low-altitude river basins in southern Europe and for the Mediterranean coasts, affecting many densely populated urban centres. We find that in these locations, the frequency of dangerous heat conditions also increases significantly faster and more strongly, and that the associated geographical pattern is robust across different models and health indicators.

Heatwaves often lead to higher morbidity and mortality predominantly in the elderly, infants and persons with pre-existing cardiovascular and respiratory disease⁷. Substantial excess mortality has been observed during several recent heatwaves^{8,9}, including the devastating summer of 2003, with around 40,000 heat-related deaths across Europe^{10,11}. The climatic factors contributing to enhanced morbidity and mortality mainly relate to a combination of extremely high day- and night-time temperatures¹², to high relative humidity^{13,14} and often to an extended duration (several days) of the heatwave^{9,15}.

Here we analyse future changes in impact-relevant summer heatwave indices based on six high-resolution regional climate models (RCMs) of the ENSEMBLES multi-model scenario experiment¹⁶. The RCMs are driven by three different general circulation model runs (see the Methods section). The findings are compared to eight RCM simulations of the previous multi-model experiment PRUDENCE (Supplementary Information). The methodology involves analysis of the statistics and spatial patterns of daily summer temperature and heatwave indices in 30-year time slices. The selected indices account for the roles of extended duration, night-time temperatures and relative humidity of heatwaves.

Temperature variability versus mean changes

Figure 1 shows simulated changes in temperature statistics for the period 2071–2100 relative to 1961–1990 (control climatology).

All six RCMs project the most pronounced mean summer warming over southernmost Europe (up to 6 K, Fig. 1a and Supplementary Fig. S2), whereas the maximum increase in daily variability is simulated further north over a zonal belt along the northern Mediterranean coasts centred at about 45°N (hereafter referred to as south-central Europe; Fig. 1b and Supplementary Fig. S3). This is consistent with the findings of the PRUDENCE simulations^{17,18} (Supplementary Fig. S1a,b). The enhanced daily temperature variability, here defined as the standard deviation across all summer days, relates to changes at interannual, seasonal and intraseasonal timescales¹⁸. Most of the RCMs analysed tend to overestimate the mean and variability of observed daily maximum temperatures¹⁹ (Table 1), a bias that has also been found for the PRUDENCE simulations²⁰.

The intensity of daily summer temperature extremes is analysed using percentiles (Fig. 1d–g). For instance, the 99th (95th) percentile roughly represents the warmest day (warmest 5 days) per season. For south-central Europe we find that (1) extreme conditions warm significantly stronger (regionally more than 50%) than mean summer temperatures (Fig. 1f,g versus Fig. 1a, more distinct in PRUDENCE; Supplementary Fig. S1) and (2) there is a distinct northward shift of the regional warming maxima from lower to higher percentiles (Fig. 1d–g). For southernmost Europe, we find a different behaviour, with extreme days warming by a similar or smaller amount than the mean. The peculiar differences between the warming of average (50th percentile) and hot days (99th percentile) are due to the variability increase (Fig. 1b). Even a small variability increase may translate into a significant change in the intensity of extremes. Thus, the analysis confirms previous studies of temperature variability changes^{1,17,18,20} and extends these results to daily temporal resolution and to a more recent set of high-resolution climate simulations (compare with PRUDENCE, Supplementary Fig. S1). We note that the implied changes in temperature statistics would have considerable effects. For instance, the 99th percentile warms regionally by more than 7 K, which implies temperature extremes that are far more intense than ever experienced in the present climate.

Although the latitude and extent of the variability changes varies across models (Supplementary Fig. S3), the associated physical mechanisms are the same. The variability changes have been found to be a combined effect of changes in atmospheric circulation and the transition from a relatively wet to dry soil moisture regime^{18,21,22}, a mechanism that has also been detected for recent heatwaves²³. Associated with the distinct soil drying and reduced evapotranspiration, all RCMs project a substantial reduction of relative humidity by up to 10–15% (Supplementary Fig. S4) collocated with the increases of temperature variability and diurnal temperature range (Fig. 1c).

¹Institute for Atmospheric and Climate Science, ETH Zurich, Universitätstr. 16, 8092 Zürich, Switzerland, ²Climate and Global Dynamics Division, National Center for Atmospheric Research (NCAR), Boulder, Colorado 80305, USA. *e-mail: erich.fischer@env.ethz.ch.

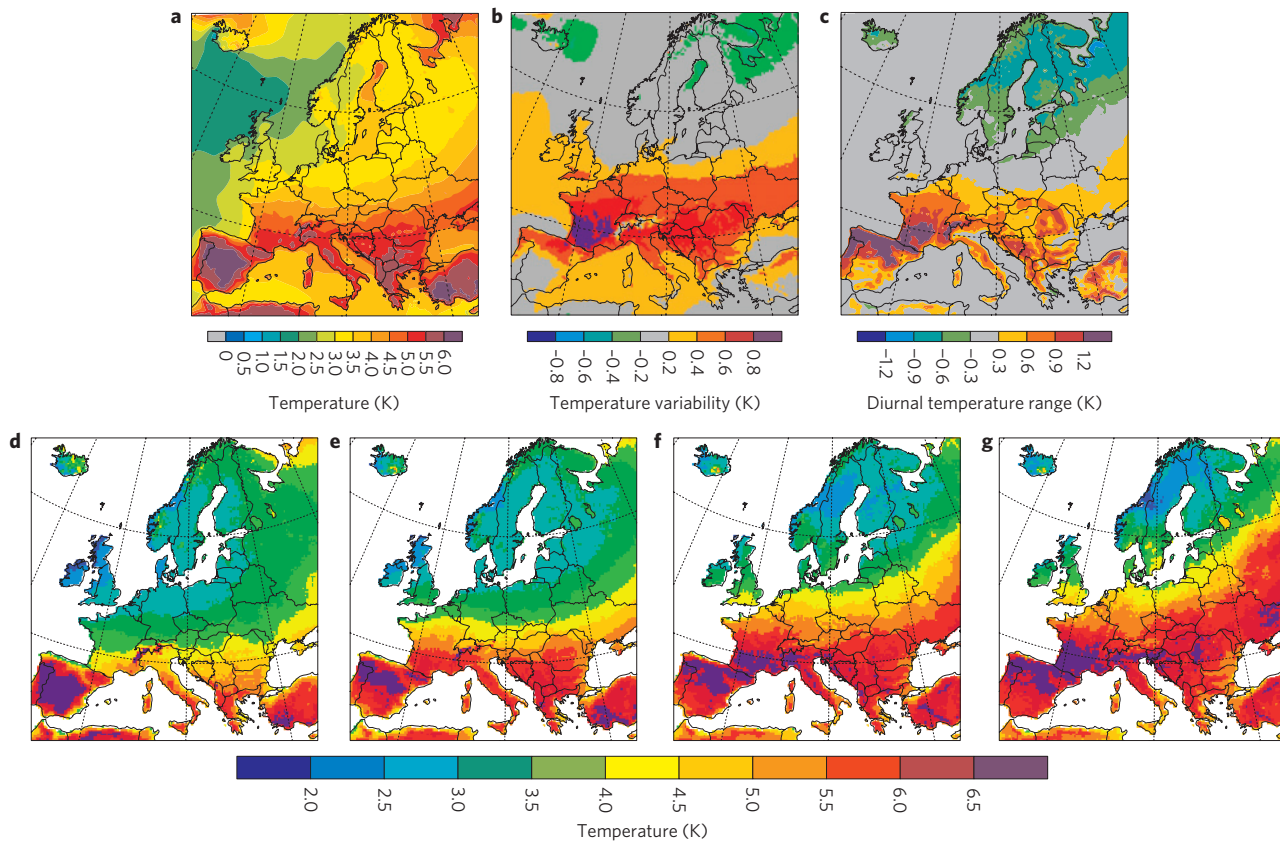


Figure 1 | Climate-change scenarios for daily summer temperature statistics. Projected ensemble mean changes in summer (JJA) for six simulations of the ENSEMBLES project for 2071–2100 with respect to 1961–1990. **a**, Mean temperature. **b**, Daily temperature variability (standard deviations of all summer days). **c**, Diurnal temperature range. **d–g**, The same as in **a**, but for 10th (**d**), 50th (**e**), 95th (**f**) and 99th (**g**) percentiles of daily maximum temperatures.

Changes in heatwave characteristics and health impacts

Most of the impacts of temperature extremes on human health relate not only to individual hot days as analysed above but are strongly affected by other factors. Thus, here we explore specific health-related heatwave indices that account for three well-known key factors: heatwave duration, night-time (minimum) temperatures and ambient humidity.

To assess changes in extended hot episodes, we define a heatwave to be a spell of at least six consecutive days with maximum temperatures exceeding the local 90th percentile of the control period (1961–1990). To quantify changes in heatwave characteristics, we differentiate heatwave day frequency (HWF90), amplitude (HWA90), number (HWN90) and maximum duration (HWD90) (see the Methods section). All of these characteristics are expected to become more severe, already by 2021–2050 and to a much stronger extent by 2071–2100.

The frequency of heatwave days (HWF90) strongly increases in the Mediterranean region (Fig. 2a,b). Averaged over the Iberian peninsula and the Mediterranean, HWF90 changes from about 2 days per average summer (1961–1990) to around 6–24 days in 2021–2050 and 27–67 days in 2071–2100 (Table 1, range depending on model). The average number of heatwaves (HWN90) increases from one every 3–5 summers (1961–1990) to about 2–3 heatwaves per season (2071–2100). Moreover, simulated heatwaves are 2–5 times longer by the end of the twenty-first century (2071–2100).

The pattern of heatwave amplitude (HWA90) changes (Fig. 2c,d) is reminiscent of that seen in the uppermost percentiles of Fig. 1f,g. This confirms the above-noted variability-induced shift between different heatwave indices: changes in heatwave frequency, number and duration mainly relate to the mean warming (maximum changes in southernmost Europe), whereas

the heatwave amplitude is most sensitive to changes in temperature variability (maximum over south-central Europe). The findings are qualitatively consistent with earlier simulations from the PRUDENCE ensemble²⁴.

In the following we focus on changes in warm nights, which are known to strongly amplify health effects by inhibiting the recovery from the daytime heat and by exacerbating the impact through sleep deprivation. The consecutive occurrence of hot days ($TMAX > 35^{\circ}\text{C}$) and tropical nights ($TMIN > 20^{\circ}\text{C}$) (hereafter referred to as combined hot days and tropical nights, CHT) has been found to explain spatial and temporal variance in excess mortality during recent heatwaves^{10,12}. The simulated CHT values (1961–1990) differ substantially between models (Table 1). As CHT relate to absolute temperature thresholds, they are particularly sensitive to biases in the model climatology. However, the spatial pattern of CHT changes, which is of particular interest here, compares remarkably well across RCMs (Supplementary Fig. S5). The highest probability of CHT (1961–1990) as well as the most pronounced projected changes are found in southern European river basins and along the Mediterranean coasts (Fig. 3a). All RCMs consistently simulate more frequent CHT (regionally a doubling by 2021–2050) and a northward expansion of the area where CHT occur (Supplementary Fig. S5).

The critical temperature thresholds for health impacts are not universal but may vary because of demographic factors (for example, age and sex), health status, socio-economic factors (for example, housing and access to air-conditioning) as well as regional acclimatization and adaptation. For instance, the critical levels are lower for the elderly and infants than for young healthy persons. Thus, we tested the robustness and found that the geographical patterns in Fig. 3a are consistent and independent of the choice of the threshold (Supplementary Fig. S8).

Table 1 | Simulated and observed temperature statistics and heatwave indices.

Region	Iberian peninsula	Mediterranean	France	Central Europe	Eastern Europe	British Isles
MEAN (°C)						
OBS	28.1	26.8	23.4	21.2	23.6	18.1
1961–1990	28.7 (31.4/26.7)	29.3 (31.8/26.4)	22.9 (24.8/20.1)	21.4 (23.6/18.5)	24.4 (27.9/21.2)	16.9 (17.3/15.7)
2021–2050	31.2 (34.5/28.8)	31.8 (34.7/28.2)	24.8 (27.6/21.5)	22.8 (25.4/19.4)	26.3 (30.2/22.2)	18.0 (19.2/16.4)
2071–2100	34.7 (37.2/32.6)	34.9 (37.3/31.5)	27.7 (30.1/24.3)	25.1 (27.8/21.4)	28.8 (32.4/24.4)	19.6 (21.1/17.5)
STD (°C)	4.0	3.5	3.8	4.0	3.8	2.8
1961–1990	4.9 (5.4/4.5)	4.7 (5.5/4.1)	4.8 (6.1/3.7)	4.5 (6.2/3.4)	4.8 (6.5/3.8)	2.9 (3.9/2.1)
2021–2050	5.0 (5.4/4.6)	4.7 (5.4/4.3)	5.0 (6.4/4.0)	4.6 (6.4/3.3)	4.9 (6.6/3.8)	3.0 (3.7/2.4)
2071–2100	5.0 (5.4/4.7)	4.9 (5.4/4.6)	5.5 (6.8/4.7)	5.1 (6.9/3.9)	5.3 (6.8/4.4)	3.3 (4.1/2.5)
95P (°C)	34.0	32.2	30.2	28.2	29.7	23.2
OBS	36.0 (38.9/33.6)	36.3 (39.1/33.3)	31.2 (35.1/27.0)	29.5 (34.0/25.1)	32.5 (37.7/28.0)	22.3 (24.3/19.9)
1961–1990	38.5 (41.8/35.8)	38.8 (41.9/35.0)	33.4 (38.2/28.6)	31.0 (36.2/25.6)	34.6 (40.5/29.0)	23.6 (25.4/21.0)
2021–2050	42.1 (44.0/39.9)	42.0 (44.0/38.7)	37.0 (41.9/32.5)	34.2 (40.2/28.7)	37.7 (42.7/32.1)	25.7 (28.6/22.4)
HWF90 (days per season)						
1961–1990	1.6 (2.2/1.2)	2.0 (2.4/1.7)	1.5 (2.4/0.7)	1.1 (1.9/0.5)	1.3 (1.8/0.9)	1.9 (2.2/1.7)
2021–2050	11.9 (17.3/8.2)	13.2 (24.1/6.0)	5.9 (8.7/3.1)	3.7 (7.6/1.6)	6.6 (13.3/2.2)	6.1 (9.2/4.7)
2071–2100	39.9 (58.0/30.3)	40.4 (67.3/27.5)	20.5 (37.0/12.2)	11.8 (17.7/6.2)	18.0 (29.9/9.0)	16.6 (38.1/7.3)
HWN90 (heatwaves per season)						
1961–1990	0.2 (0.3/0.2)	0.3 (0.3/0.2)	0.2 (0.3/0.1)	0.1 (0.2/0.1)	0.2 (0.2/0.1)	0.2 (0.3/0.2)
2021–2050	1.3 (1.7/1.0)	1.4 (2.2/0.7)	0.7 (0.9/0.4)	0.4 (0.8/0.2)	0.7 (1.3/0.3)	0.7 (1.0/0.5)
2071–2100	3.0 (3.2/2.5)	2.9 (3.2/2.6)	2.0 (3.1/1.4)	1.3 (2.0/0.8)	1.7 (2.5/1.1)	1.6 (3.0/0.9)
HWA90 (°C)						
1961–1990	37.8 (40.7/35.6)	38.6 (40.9/35.9)	34.0 (38.5/29.8)	32.9 (37.1/27.9)	35.2 (39.8/30.7)	25.6 (28.4/22.6)
2021–2050	40.2 (43.1/37.5)	40.4 (43.1/36.9)	35.9 (41.3/31.2)	33.8 (39.0/28.5)	36.8 (42.1/31.7)	26.1 (28.4/22.9)
2071–2100	43.7 (45.8/41.5)	43.5 (45.6/40.2)	39.2 (44.5/34.4)	36.6 (42.6/31.1)	39.7 (44.7/34.0)	27.9 (31.1/24.2)
HWD90 (days)						
1961–1990	7.9 (8.6/7.4)	7.7 (8.6/7.0)	7.9 (9.1/7.2)	7.5 (8.4/6.7)	7.5 (8.1/6.7)	7.8 (8.3/7.4)
2021–2050	10.4 (12.0/9.2)	10.9 (14.1/9.0)	9.4 (10.6/8.0)	8.3 (10.1/7.1)	9.2 (12.4/7.5)	9.4 (10.1/8.8)
2071–2100	20.3 (31.4/16.7)	22.0 (43.5/14.2)	12.8 (18.1/9.9)	10 (13.6/8.1)	12.2 (16.9/8.7)	11.9 (19.9/8.5)
CHT (days per season)						
1961–1990	8.2 (14.0/2.1)	10.2 (17.6/1.6)	1.4 (3.9/0.0)	0.4 (1.3/0.0)	3.6 (9.6/0.3)	0.0 (0.0/0.0)
2021–2050	19.0 (28.3/6.3)	22.3 (34.7/3.8)	4.3 (10.4/0.2)	1.6 (4.9/0.0)	8.7 (18.9/0.9)	0.0 (0.1/0.0)
2071–2100	38.6 (56.3/22.8)	41.0 (58.2/13.9)	11.7 (21.5/2.2)	4.9 (12.6/0.1)	17.1 (29.7/3.7)	0.2 (0.8/0.0)
AT105F (days per season)						
1961–1990	1.6 (5.9/0.0)	1.6 (7.2/0.1)	0.6 (3.1/0.0)	0.5 (3.1/0.0)	1.0 (5.3/0.0)	0.0 (0.1/0.0)
2021–2050	5.3 (16.1/0.2)	5.5 (18.4/0.4)	2.0 (8.1/0.0)	1.2 (6.1/0.0)	2.7 (11.7/0.0)	0.0 (0.2/0.0)
2071–2100	15.8 (30.6/4.5)	16.2 (32.3/3.2)	5.8 (14.6/0.4)	3.2 (11.1/0.0)	7.0 (18.9/0.4)	0.1 (0.6/0.0)

Regional averages are shown for JJA mean temperature (MEAN), daily variability expressed as standard deviation (STD) and 95th percentile (95P) of daily summer temperatures, heatwave day frequencies (HWF90), heatwave number (HWN90), heatwave amplitude (HWA90), heatwave duration (HWD90), combined occurrence of hot days and tropical nights (CHT) and frequency of apparent temperatures (heat indices) exceeding 40.6 °C/105F (AT105F). Observations (OBS) are based on daily gridded observations for the period 1961–1990 (ref. 19). Values are averaged over the land points of the following six European standard PRUDENCE regions (Supplementary Information). For each period, the ensemble mean (first number) as well as the minimum and maximum ensemble member (in parentheses) are listed.

Last, we consider the role of humidity, a well-established health factor¹³. Future changes in relative humidity may in principle either amplify or offset the health effects of temperature extremes. To account for this effect, the daily maximum apparent (human-perceived) temperature (hereafter AT, often referred to as heat index) is calculated. This represents a combined measure of temperature and humidity stress under shaded conditions¹⁴ (see the Methods section). High relative humidity is a particularly relevant stress factor for human thermoregulation. Humans normally control their body temperature by sweating (evaporative cooling). When the relative humidity is high, the evaporation rate is reduced, thereby reducing the effectiveness of this mechanism.

Here, we analyse changes in the frequency of AT higher than 40.6 °C (105 °F, hereafter AT105F), the threshold at which the US National Weather Service issues a heat advisory because of dangerous health conditions (high incidence of heat cramps, heat

exhaustion and heat strokes). Note that such extreme thresholds are rarely exceeded in the control period (Table 1). The simulated AT105F differ strongly between RCMs in current as well as in future climatic conditions, owing to differences in both relative humidity and temperatures. It is difficult to validate AT, owing to the lack of daily minimum relative humidity observations. However, most of the RCMs have a negative relative humidity bias with respect to observed seasonal means²⁵, and a positive temperature bias over southern Europe (especially the RCMs driven by HadCM3).

All RCMs consistently simulate higher AT105F at the end of the twenty-first century (Fig. 3b, Supplementary Fig. S6) even over regions of substantially reduced relative humidity (Supplementary Fig. S4). Drier conditions regionally dampen but in no way offset the health effects of elevated temperatures (interior parts of the Iberian peninsula, of southern France, the Balkans and Turkey). This is consistent with an earlier study based on a single

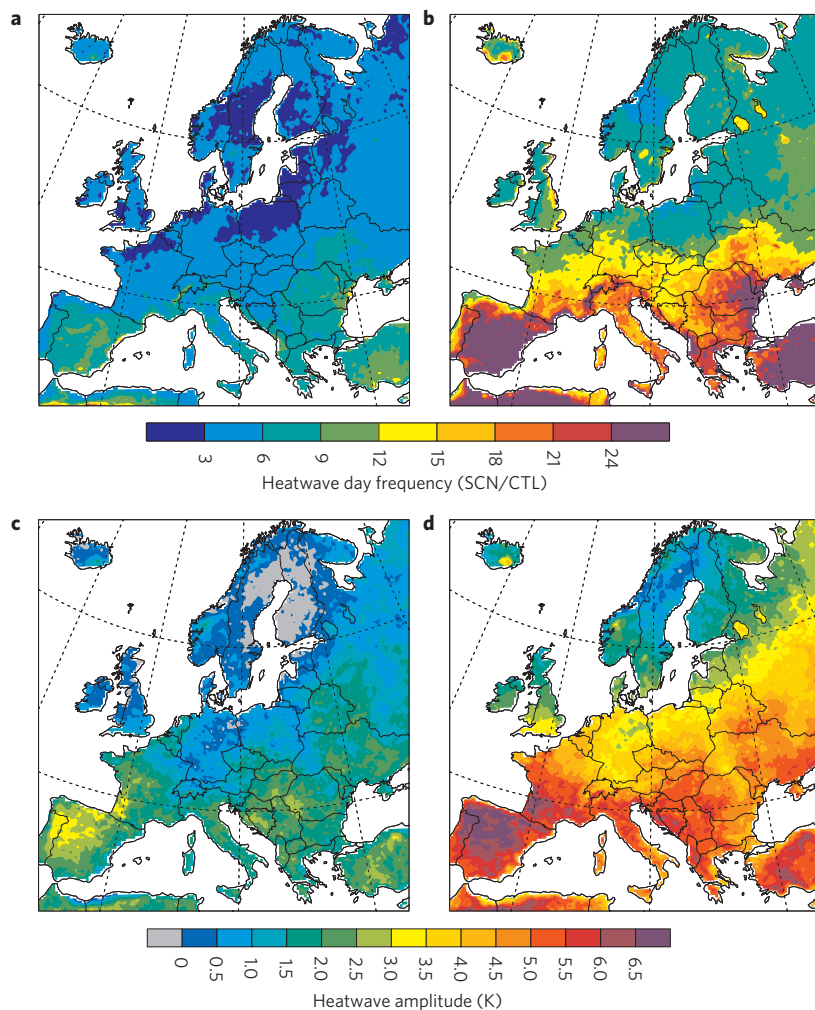


Figure 2 | Heatwave frequency and amplitude. **a-d**, The same as in Fig. 1, but for projected ensemble-mean changes of heatwave day (HWF90) frequency expressed as ratio between scenario and control period (SCN/CTL) (**a,b**) and changes in heatwave amplitude (HWA90) expressed in degrees Celsius (**c,d**). Changes are shown for 2021–2050 (**a,c**) and 2071–2100 (**b,d**) with respect to 1961–1990.

model simulation²⁶. Despite considerable uncertainties regarding the exact magnitude of the changes and the representation of feedback mechanisms in climate models^{27,28}, the spatial patterns compare remarkably well across models and strongly resemble the CHT patterns: the largest AT changes are projected along the Mediterranean coasts and in southern European river basins such as the Po and lower Danube basin (see Supplementary Fig. S12 for geographical terms). We do not only find remarkable agreement across models, but also across different AT thresholds (37.8 or 35 °C) (Supplementary Fig. S9) and even across different health indices accounting for the combined effect of temperature and humidity (HUMIDEX, Supplementary Fig. S10 and approximated wet bulb globe temperature, Supplementary Fig. S11).

The surprisingly robust nature of the detected geographical patterns ultimately rests on two factors. First, the same change in mean AT results in a stronger threshold exceedance for high climatological AT105 (refs 18,26). Second, the nonlinearity of health indices implies that high base temperatures and humidity yield higher AT changes with equal warming²⁹. This effect amplifies the current pattern of temperature extremes. As temperature exhibits a strong gradient with altitude (in average $-0.6 \text{ K}/100 \text{ m}$), the nonlinearity pinpoints the low-altitude regions (coasts and large river basins) and mirrors the topography. Moreover, owing to the proximity of adjacent seas, the simulated reduction in daily minimum relative humidity is comparatively

small along the coasts (Supplementary Fig. S4), further amplifying the effect in these regions. Note that the definition of apparent temperature used here neglects possible health effects of air pollution, wind, radiation and clouds. Furthermore, we do not account for changes in vulnerability, (for example, changes in age structure or acclimatization) or the role of mitigation strategies (implementation of heat warning systems or air-conditioning), which have potentially important effects on future health impacts associated with climate change.

Our results yield a robust estimate of the regions that might be most seriously affected. Given the high consistency of the detected geographical patterns across different models and health indices, the projections seem alarming. Some of the most densely populated European regions, such as the urban areas of Athens, Bucharest, Marseille, Milan, Rome and Naples, would experience the severest changes in health indicators. The health risk might even be underestimated here, because current models do not represent the amplifying effects of urban heat islands.

Methods

We analyse daily output of a transient ensemble of RCM experiments carried out within the European project ENSEMBLES. The RCM simulations were run over the entire European continent at a horizontal resolution of about 25 km. We analyse the six simulations available at the time of analysis, which cover the full period 1950–2100 (1950–2099 in the case of the three RCMs driven by HadCM3) and provide all of the necessary temperature and humidity fields at daily resolution.

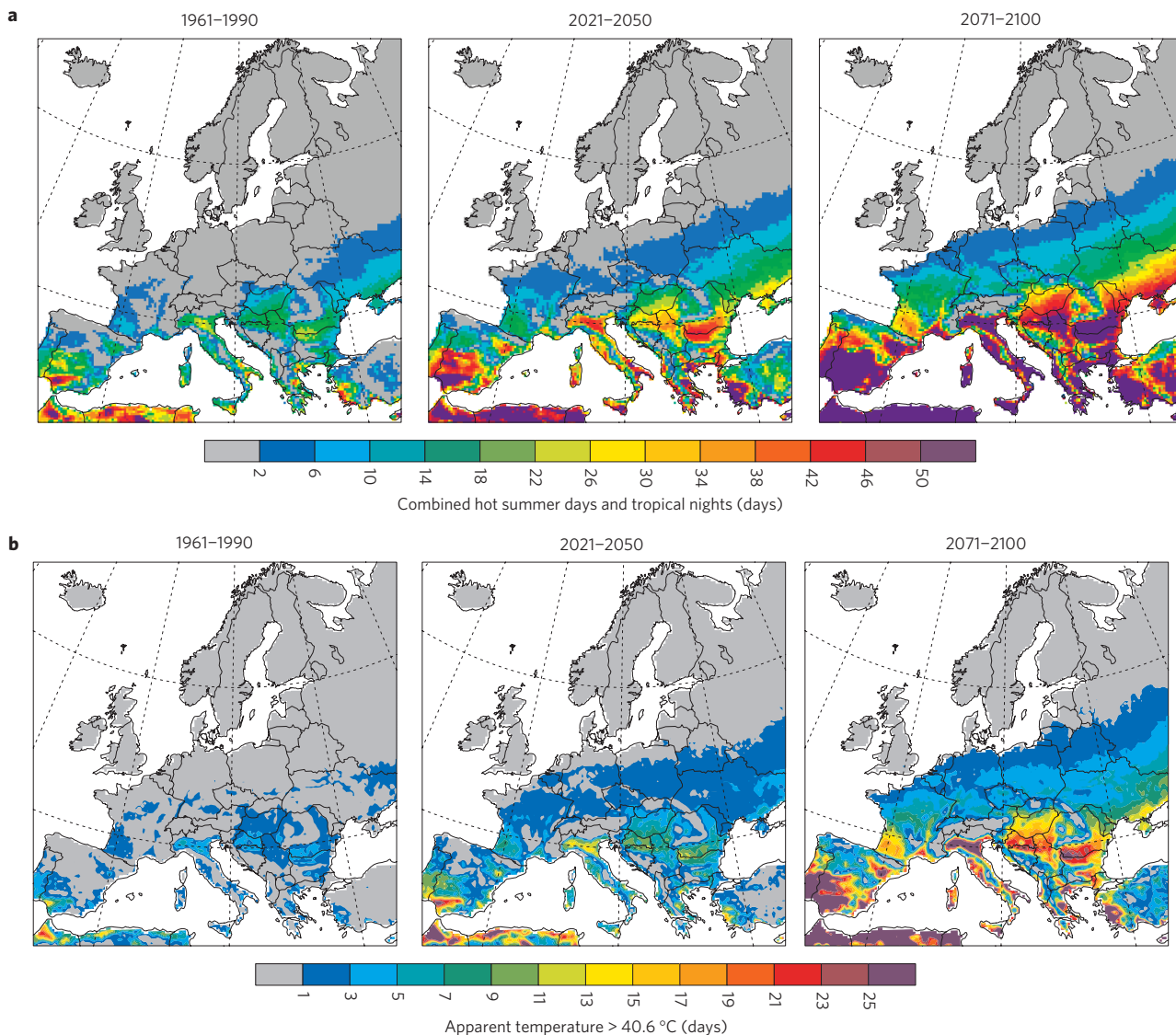


Figure 3 | Increasing health risk. **a,b**, The same as in Fig. 1, but for projected ensemble mean of average number of combined hot summer days ($TMAX > 35^{\circ}\text{C}$) and tropical nights ($TMIN > 20^{\circ}\text{C}$) (**a**) and average number of summer days exceeding the apparent temperature (heat index) threshold of 40.6°C (105°F) (**b**).

This includes the following six RCMs: Community Climate Change Consortium for Ireland (C4I) with the RCA3 model, ETH Zurich Switzerland (ETH) with the COSMO-CLM model, UK Met Office Hadley Centre (HC) with the HadRM model, Royal Netherlands Meteorological Institute (KNMI) with the RACMO model, Max Planck Institute (MPI) with the REMO model, the Swedish Meteorological and Hydrological Institute (SMHI) with the RCA model. Details on these models may be found at <http://ensemblesrt3.dmi.dk>. The C4I, ETH and HC models have been driven by lateral boundary conditions of two HadCM3 global climate models (HadCM3Q0 for ETH and HC, and HadCM3Q16 for C4I) and the MPI, KNMI and SMHI simulations with the ECHAM5 model. All simulations were forced with the SRES A1B greenhouse gas and aerosol scenario. The RCM output is analysed for the three time slices 1961–1990, 2021–2050 and 2071–2100 (or 2070–2099, depending on availability).

We apply three types of analysis. First, we analyse the statistical distribution of daily summer (June–August) temperatures for all simulations and grid points. This is based on local percentiles of temperature distributions and is conducted for daily minimum and maximum temperatures, as well as the diurnal temperature range. The analysis is carried out for all models and grid points individually before ensemble and area averaging.

Second, we analyse multi-day heatwaves. Here a heatwave is defined as a spell of at least six consecutive days with maximum temperatures exceeding the local 90th percentile of the control period (1961–1990). To account for the seasonal cycle, the 90th percentile is calculated for each calendar day, each model and at each grid point using a centred 15-day-long time window. On the basis of this

definition, the following extreme summer (JJA) temperature indices are derived for 30-year time slices.

HWF90 (heatwave day frequency): the average frequency of days meeting the heatwave criterion.

HWN90 (number of heatwaves): the average number of heatwaves per summer.

HWA90 (heatwave amplitude): the average peak temperature of the hottest heatwave per summer (years without heatwaves are excluded from this analysis).

HWD90 (heatwave duration): the average duration of the longest heatwave per summer (years without heatwaves are excluded from this analysis).

Third, we analyse indices that are known to be particularly important in relation to health impacts, using absolute (location-independent) definitions. We consider the following.

CHT (combined hot days and tropical nights): the average number of summer days with maximum temperatures exceeding 35°C and minimum temperatures exceeding 20°C .

AT105F (exceedance of apparent temperature threshold): the average number of summer days with maximum humidity-corrected AT exceeding 40.6°C (105°F). The apparent temperature (often referred to as the heat index; refs 14,30) represents heat stress on the human body by accounting for the effects of environmental factors beyond temperature and by representing the nonlinear nature of heat stress. There are many different versions of apparent temperature. Here we use an approximated version that accounts for ambient humidity under shaded conditions and that is commonly used by NOAA in North America (see

<http://www.crh.noaa.gov/pub/heat.php>), but we use a definition in degrees Celsius rather than degrees Fahrenheit:

$$AT = c_1 + c_2 T + c_3 T^2 + RH(c_4 + c_5 T + c_6 T^2) + RH^2(c_7 + c_8 T + c_9 T^2)$$

Here T is daily maximum temperature in degrees Celsius, RH the simultaneous relative humidity in % and the coefficients are defined as $c_1 = -8.7847$, $c_2 = 1.6114$, $c_3 = -0.012308$, $c_4 = 2.3385$, $c_5 = -0.14612$, $c_6 = 2.2117 \times 10^{-3}$, $c_7 = -0.016425$, $c_8 = 7.2546 \times 10^{-4}$, $c_9 = -3.582 \times 10^{-6}$.

Ideally the apparent temperature is calculated from the daily maximum temperature and the simultaneous relative humidity. As the latter is not available for our database, we use the daily minimum relative humidity, which at first approximation coincides with the maximum temperature in the diurnal cycle. The use of daily mean relative humidity instead results in substantially higher values, which explains the main differences between our and previous studies.

Received 11 January 2010; accepted 13 April 2010; published online 16 May 2010

References

1. Schär, C. *et al.* The role of increasing temperature variability in European summer heatwaves. *Nature* **427**, 332–336 (2004).
2. Meehl, G. A. & Tebaldi, C. More intense, more frequent, and longer lasting heat waves in the 21st century. *Science* **305**, 994–997 (2004).
3. Beniston, M. The 2003 heat wave in Europe: A shape of things to come? An analysis based on Swiss climatological data and model simulations. *Geophys. Res. Lett.* **31**, L02202 (2004).
4. Clark, R. T., Brown, S. J. & Murphy, J. M. Modeling Northern Hemisphere summer heat extreme changes and their uncertainties using a physics ensemble of climate sensitivity experiments. *J. Clim.* **19**, 4418–4435 (2006).
5. Klein, T. A., Können, G. & Seltzer, F. Signals of anthropogenic influence on European warming as seen in the trend patterns of daily temperature variance. *Int. J. Climatol.* **25**, 1–16 (2005).
6. Della-Marta, P. M. *et al.* Doubled length of Western European summer heat waves since 1880. *J. Geophys. Res.* **112**, D15103 (2007).
7. Basu, R. & Samet, J. M. Relation between elevated ambient temperature and mortality: A review of the epidemiologic evidence. *Epidemiol. Rev.* **24**, 190–202 (2002).
8. Semenza, J. *et al.* Heat-related deaths during the July 1995 heat wave in Chicago. *N. Engl. J. Med.* **335**, 84–90 (1996).
9. Changnon, S. A., Kunkel, K. E. & Reinke, B. C. Impacts and responses to the 1995 heat wave: A call to action. *Bull. Am. Meteorol. Soc.* **77**, 1497–1506 (1996).
10. Hémon, D. *et al.* Surmortalité liée à la canicule d'août 2003 en France. *Bull. Épidémiol. Hebd.* **45–46**, 1–5 (2003).
11. García-Herrera, R., Díaz, J., Trigo, R. M., Luterbacher, J. & Fischer, E. M. A review of the European summer heatwave of 2003. *Crit. Rev. Environ. Sci. Technol.* **40**, 267–306.
12. Grize, L., Huss, A., Thommen, O., Schindler, C. & Braun-Fahrlander, C. Heat wave 2003 and mortality in Switzerland. *Swiss Med. Wkly* **135**, 200–205 (2005).
13. Conti, S. *et al.* Epidemiologic study of mortality during the summer 2003 heat wave in Italy. *Environ. Res.* **98**, 390–399 (2005).
14. Steadman, R. G. The assessment of sultriness. Part I: A temperature-humidity index based on human physiology and clothing science. *J. Appl. Meteorol.* **18**, 861–873 (1979).
15. Trigo, R. M. *et al.* Evaluating the impact of extreme temperature based indices in the 2003 heatwave excessive mortality in Portugal. *Environ. Sci. Policy* **12**, 844–854 (2009).
16. Christensen, J. H., Boberg, F., Christensen, O. B. & Lucas-Picher, P. On the need for bias correction of regional climate change projections of temperature and precipitation. *Geophys. Res. Lett.* **35**, L20709 (2008).
17. Giorgi, F., Bi, X. & Pal, J. Mean, interannual variability and trends in a regional climate change experiment over Europe. II: Climate change scenarios (2071–2100). *Clim. Dynam.* **23**, 839–858 (2004).
18. Fischer, E. M. & Schär, C. Future changes in daily summer temperature variability: Driving processes and role for temperature extremes. *Clim. Dynam.* **33**, 917–935 (2009).
19. Haylock, M. R. *et al.* A European daily high-resolution gridded dataset of surface temperature and precipitation for 1950–2006. *J. Geophys. Res.* **113**, D20119 (2008).
20. Kjellström, E. *et al.* Modelling daily temperature extremes: Recent climate and future changes over Europe. *Clim. Change* **81**, 249–265 (2007).
21. Seneviratne, S. I., Lüthi, D., Litschi, M. & Schär, C. Land–atmosphere coupling and climate change in Europe. *Nature* **443**, 205–209 (2006).
22. van Ulden, A., Lenderink, G., van den Hurk, B. & van Meijgaard, E. Circulation statistics and climate change in Central Europe: PRUDENCE simulations and observations. *Clim. Change* **81**, 179–192 (2007).
23. Fischer, E. M., Seneviratne, S. I., Vidale, P. L., Lüthi, D. & Schär, C. Soil moisture–atmosphere interactions during the 2003 European summer heatwave. *J. Clim.* **20**, 5081–5099 (2007).
24. Koffi, B. & Koffi, E. Modelling of heat waves in Europe. *Clim. Res.* **36**, 153–168 (2008).
25. Willett, K. W., Jones, P. D., Gillett, N. P. & Thorne, P. W. Recent changes in surface humidity: Development of the HadCRUH dataset. *J. Clim.* **21**, 5364–5383 (2008).
26. Diffenbaugh, N. S., Pal, J. S., Giorgi, F. & Gao, X. Heat stress intensification in the Mediterranean climate change hotspot. *Geophys. Res. Lett.* **34**, L11706 (2007).
27. Hohenegger, C., Brockhaus, P., Bretherton, C. S. & Schär, C. The soil moisture–precipitation feedback in simulations with explicit and parameterized convection. *J. Clim.* **22**, 5003–5020 (2009).
28. Buser, C. M., Künsch, H. R., Lüthi, D., Wild, M. & Schär, C. Bayesian multi-model projection of climate: Bias assumptions and interannual variability. *Clim. Dynam.* **33**, 849–868 (2009).
29. Delworth, T. L., Mahlman, J. D. & Knutson, T. R. Changes in heat index associated with CO₂-induced global warming. *Clim. Change* **43**, 369–386 (1999).
30. Karl, T. R. & Knight, R. W. The 1995 Chicago heat wave: How likely is a recurrence? *Bull. Am. Meteorol. Soc.* **78**, 1107–1119 (1997).

Acknowledgements

This research was supported by the Swiss National Science Foundation (NCCR Climate) and by the ENSEMBLES project, funded by the European Commission's 6th Framework Programme (contract GOCE-CT-2003-505539). Computational resources for the ETH climate simulations have been provided by the Swiss Center for Scientific Computing (CSCS).

Author contributions

Both authors contributed extensively to the work presented in this letter.

Additional information

The authors declare no competing financial interests. Supplementary information accompanies this paper on www.nature.com/naturegeoscience. Reprints and permissions information is available online at <http://npg.nature.com/reprintsandpermissions>. Correspondence and requests for materials should be addressed to E.M.F.